

Approximations of the Iterative Stockholder Analysis scheme using exponential basis functions

YingXing Cheng and Benjamin Stamm*

*Institute of Applied Analysis and Numerical Simulation, University of Stuttgart, Pfaffenwaldring
57, 70569, Stuttgart, Germany*

E-mail: benjamin.stamm@mathematik.uni-stuttgart.de

Abstract

In this work, we introduce several approximations of the Iterative Stockholder Analysis (ISA) method based on exponential basis functions. These approximations are categorized into linear and non-linear models, referred to as LISA and NLIS, respectively. By particular choices of hyperparameters in the NLIS model, both LISA and the Minimal-Basis Iterative Stockholder (MBIS) method can be reproduced. Four LISA variants are constructed using systematically generated exponential basis functions derived from the NLIS model applied to atomic systems. The performance of these LISA variants and NLIS models is benchmarked on 15 small molecules, including neutral, anionic, and cationic species. To facilitate comparison, we propose several metrics designed to highlight differences between the methods. Our results demonstrate that LISA, employing Gaussian basis functions derived from the NLIS model on isolated atomic systems, achieves an optimal balance of computational accuracy, robustness, and efficiency, particularly in minimizing the objective function.

1 Introduction

Defining an atom in a multi-atom molecule remains an open question in chemistry. This is because the partitioning of molecular orbitals or electron density into atomic contributions is not an intrinsic property in quantum mechanics. Consequently, different partitioning methods can yield significantly different atom-in-molecule (AIM) properties, such as atomic charges and multipole moments, which are crucial for developing molecular polarizable force fields.^{1–19} The classification and comparison of these methods have been discussed extensively in the recent studies^{20–30} and references therein.

In this work, we focus on the Iterative Stockholder Analysis (ISA) family of methods.^{21,22} The ISA method employs the Kullback–Leibler entropy as an objective functional to minimize the dissimilarity between the AIM electron density and the reference proatomic electron densities, subject to the constraint that the sum of the proatomic densities, also known as the promolecular density, equals the molecular electron density. In the original ISA method,^{21,22} the proatomic density corresponds to the spherical average of the AIM density.

Although the solution of the ISA method is analytically unique and convex,³⁰ it is not numerically robust, and the spherical average of the AIM or proatomic density does not monotonically decay in certain systems, which is counterintuitive in the chemistry community.²⁴ To address these numerical challenges, Verstraelen *et al.* developed an ISA variant known as GISA. In this approach, the proatomic density is approximated using a set of normalized *s*-type Gaussian basis functions with unknown non-negative expansion coefficients.²⁴ These coefficients are optimized via least-squares fitting to the proatomic density from ISA, subject to the constraint that the population of the AIM density equals that of the proatomic density. However, the quadratic objective function in GISA leads to over-delocalized proatomic densities, resulting in unphysical charges. Furthermore, atomic charges derived from GISA are not highly transferable, and conformational stability is low.²⁹

To resolve the issue of unphysical proatomic density tails, Misquitta *et al.* proposed a variant, BS-ISA, that combines Gaussian functions for short-range contributions with Slater functions for long-range behavior. Subsequently, Verstraelen *et al.* introduced another variant, MBIS, which uses a minimal set of Slater functions with unknown non-negative expansion coefficients and corresponding exponents.²⁸ The MBIS method also employs the Kullback–Leibler entropy as the objective function, subject to constraints similar to GISA. While MBIS significantly improves upon GISA and performs well in chemical applications, excessively negative atomic charges are observed in molecular anions, likely due to the limited number of Slater basis functions.²⁹

Another ISA variant, AVH, utilizes densities from selected states of isolated atoms and ions as basis functions.^{31,32} Unlike other ISA variants, AVH basis functions are not analytic. Later, Benda *et al.* proposed a unified framework for all ISA variants. These methods can be classified as linear or nonlinear ISA approximations (LISA and NLIS, respectively) based on whether nonlinear parameters are included in the basis functions to be optimized. LISA models, such as ISA, GISA, and AVH, exhibit advantageous mathematical properties, including uniqueness, convexity, and guaranteed convergence, while NLIS models, such as BS-ISA and MBIS, lack these guarantees.

A new LISA model with Gaussian basis functions similar to GISA has also been proposed in Ref. 30, with the key difference being the use of Kullback–Leibler entropy for optimizing expansion coefficients. Recently, we investigated the numerical performance of LISA models and found that LISA with Gaussian basis functions achieves lower entropy compared to GISA and MBIS, except for certain molecular anions with hydrogen atoms where MBIS performs better. This can be addressed by incorporating more diffuse Gaussian functions for hydrogen atoms in LISA, although its suitability for chemical applications remains an open question. A systematic approach to constructing basis functions is still needed, and this work aims to address this gap.

In this work, we focus exclusively on ISA variants employing exponential basis functions. We derive an NLIS model by treating expansion coefficients, exponents, and the order of the exponential basis functions as unknown parameters. The resulting stationary equations resemble

those in MBIS but include an additional equation for the order of the exponential basis functions. By imposing further simplifications, we propose several NLIS models, including a reproduction of the MBIS model by fixing the order to one and the number of basis functions to the number of rows for each element in the periodic table. Additionally, we propose a generalized MBIS model using exponential basis functions with orders ranging from one to two and the same number of basis functions as in MBIS.

Furthermore, we introduce LISA models combining Gaussian and/or Slater functions, with the exponents of exponential basis functions determined using NLIS models to fit atomic data. These models are benchmarked using 15 small molecules, including anions, cations, and neutral molecules. Four boron wheel molecules with delocalized bonding environments are also included.

In Section 2, we describe the relevant methodology for this study. Section 3 provides computational details. Results and discussions are presented in Section 4, and a summary is given in Section 5. Atomic units are used throughout.

2 Methods

2.1 ISA partitioning methods

The information loss when AIM densities are approximated by proatomic functions is modeled using the Kullback–Leibler entropy,

$$s_{\text{KL}}(\rho_a|\rho_a^0) = \int_{\mathbb{R}^3} \rho_a(\mathbf{r}) \ln \left(\frac{\rho_a(\mathbf{r})}{\rho_a^0(\mathbf{r})} \right) d\mathbf{r}, \quad (1)$$

using the conventions

$$0 \cdot \ln \left(\frac{0}{0} \right) = 0, \quad p \cdot \ln \left(\frac{p}{0} \right) = \infty \quad \forall p > 0, \quad 0 \cdot \ln \left(\frac{0}{p} \right) = 0, \quad (2)$$

where $\rho_a^0(\mathbf{r})$ and $\rho_a(\mathbf{r})$ are the proatom and AIM densities of atom a , respectively. Thus, the information loss when AIM densities are approximated by proatoms in a molecule with N_{atoms} atoms can be expressed as the sum of Kullback–Leibler entropies for each atom:

$$S(\{\rho_a\}, \{\rho_a^0\}) = \sum_{a=1}^{N_{\text{atoms}}} s_{\text{KL}}(\rho_a | \rho_a^0). \quad (3)$$

In practice, several constraints are imposed to ensure that the partitioning results align with chemical and physical properties. First, the sum of AIM densities must equal the total density $\rho(\mathbf{r})$:

$$\sum_{a=1}^{N_{\text{atoms}}} \rho_a(\mathbf{r}) = \rho(\mathbf{r}). \quad (4)$$

Second, the population of each proatom and its corresponding AIM density should be equal, avoiding ambiguity in the statistical interpretation of Eq. (3):^{28,33}

$$N_a = \int_{\mathbb{R}^3} \rho_a(\mathbf{r}) d\mathbf{r} = \int_{\mathbb{R}^3} \rho_a^0(\mathbf{r}) d\mathbf{r}. \quad (5)$$

The Lagrangian for the problem is defined as follows:

$$\begin{aligned} L[\{\rho_a\}, \lambda(\mathbf{r}), \{\rho_a^0\}] &= \sum_{a=1}^{N_{\text{atoms}}} \int_{\mathbb{R}^3} \rho_a(\mathbf{r}) \ln \left(\frac{\rho_a(\mathbf{r})}{\rho_a^0(\mathbf{r})} \right) d\mathbf{r} \\ &+ \int_{\mathbb{R}^3} \lambda(\mathbf{r}) \left(\sum_{a=1}^{N_{\text{atoms}}} \rho_a(\mathbf{r}) - \rho(\mathbf{r}) \right) d\mathbf{r} \\ &+ \sum_{a=1}^{N_{\text{atoms}}} \mu_a \left(\int_{\mathbb{R}^3} (\rho_a^0(\mathbf{r}) - \rho_a(\mathbf{r})) d\mathbf{r} \right), \end{aligned} \quad (6)$$

where $\lambda(\mathbf{r})$ is the Lagrange multiplier associated with the first constraint, and μ_a are Lagrange multipliers associated with the consistency between the proatom and AIM populations. Solving

the Euler-Lagrange equations of Eq. (6) leads to the well-known stockholder partitioning formula:

$$\rho_a(\mathbf{r}) = \rho(\mathbf{r}) \frac{\rho_a^0(\mathbf{r})}{\rho^0(\mathbf{r})}, \quad (7)$$

$$\rho^0(\mathbf{r}) = \sum_b \rho_b^0(\mathbf{r}), \quad (8)$$

where $\rho^0(\mathbf{r})$ is also referred to as the pro-molecule density.

2.2 Exponential-type basis functions

Different choices of basis functions to discretize $\rho_a^0(\mathbf{r})$ lead to different variants of the ISA method. In this work, we introduce m_a positive basis functions $g_{a,k}$ for each site \mathbf{R}_a , centered at \mathbf{R}_a and radially symmetric. Although \mathbf{R}_a can represent an arbitrary expansion center, as pointed out in Ref. 30, this work focuses on cases where \mathbf{R}_a denotes the position of the nucleus with index a . Moreover, we assume, without loss of generality, that $g_{a,k}(\mathbf{r})$ is normalized such that

$$\int_{\mathbb{R}^3} g_{a,k}(\mathbf{r}) d\mathbf{r} = 1, \quad (9)$$

and we focus on exponential functions of the following form:

$$g_{a,k}(\mathbf{r}) = \frac{n_{a,k} \alpha_{a,k}^{3/n_{a,k}}}{4\pi\Gamma(3/n_{a,k})} e^{-\alpha_{a,k}|\mathbf{r}-\mathbf{R}_a|^{n_{a,k}}}. \quad (10)$$

Here, a and k denote the indices of atoms and basis functions, respectively. For Gaussian basis functions, there holds $n_{a,k} = 2$ for all a and k , while for Slater basis functions, $n_{a,k} = 1$, corresponding to

$$g_{a,k}(\mathbf{r}) = \left(\frac{\alpha_{a,k}}{\pi}\right)^3 e^{-\alpha_{a,k}|\mathbf{r}-\mathbf{R}_a|^2}, \quad (11)$$

and

$$g_{a,k}(\mathbf{r}) = \frac{\alpha_{a,k}^3}{8\pi} e^{-\alpha_{a,k}|\mathbf{r}-\mathbf{R}_a|}, \quad (12)$$

respectively.

2.3 General Lagrangian formulation

By discretizing the proatom densities using general exponential basis functions, the discretized version of the Lagrangian in Eq. (6) can be rewritten as presented in Ref. 28:

$$\begin{aligned} L[\{\rho_a\}, \lambda(\mathbf{r}), \{c_{a,k}\}, \{\alpha_{a,k}\}, \{n_{a,k}\}, \{\mu_a\}] = & \sum_{a=1}^{N_{\text{atoms}}} \int_{\mathbb{R}^3} \rho_a(\mathbf{r}) \ln \left(\frac{\rho_a(\mathbf{r})}{\rho_a^0(\mathbf{r})} \right) d\mathbf{r} \\ & + \int_{\mathbb{R}^3} \lambda(\mathbf{r}) \left(\sum_{a=1}^{N_{\text{atoms}}} \rho_a(\mathbf{r}) - \rho(\mathbf{r}) \right) d\mathbf{r} \\ & + \sum_{a=1}^{N_{\text{atoms}}} \mu_a \left(\int_{\mathbb{R}^3} (\rho_a^0(\mathbf{r}) - \rho_a(\mathbf{r})) d\mathbf{r} \right), \quad (13) \end{aligned}$$

with

$$\rho_a^0(\mathbf{r}) = \sum_k \rho_{a,k}^0(\mathbf{r}), \quad (14)$$

$$\rho_{a,k}^0(\mathbf{r}) = c_{a,k} g_{a,k}(\mathbf{r}). \quad (15)$$

Independent variation of the Lagrangian L with respect to each variable $(\rho_a(\mathbf{r}), c_{a,k}, \alpha_{a,k}, n_{a,k})$ leads to a set of Euler-Lagrange equations, which, together with the constraints, determine the AIM and proatom densities, as well as the Lagrange multipliers $\lambda(\mathbf{r})$ and $\{\mu_a\}$.

2.3.1 Derivative with respect to $c_{a,k}$

First, consider the derivative of L with respect to $c_{a,k}$.²⁸

$$0 = \frac{\partial L}{\partial c_{a,k}} = \int_{\mathbb{R}^3} \frac{\delta L}{\delta \rho_a^0(\mathbf{r})} \frac{\partial \rho_a^0(\mathbf{r})}{\partial c_{a,k}} d\mathbf{r} \quad (16)$$

$$= \int_{\mathbb{R}^3} \left(-\frac{\rho_a(\mathbf{r})}{\rho_a^0(\mathbf{r})} + \mu_a \right) g_{a,k}(\mathbf{r}) d\mathbf{r} \quad (17)$$

$$= \mu_a - \int_{\mathbb{R}^3} \frac{\rho_a(\mathbf{r})}{\rho_a^0(\mathbf{r})} g_{a,k}(\mathbf{r}) d\mathbf{r}. \quad (18)$$

Multiplying by $c_{a,k}$ and summing over the shells k of atom a , using Eq. (5), we obtain,

$$0 = \sum_k c_{a,k} \frac{\partial L}{\partial c_{a,k}} = \mu_a N_a^0 - \int_{\mathbb{R}^3} \frac{\rho_a(\mathbf{r})}{\rho_a^0(\mathbf{r})} \sum_k c_{a,k} g_{a,k}(\mathbf{r}) d\mathbf{r} \quad (19)$$

$$= \mu_a N_a^0 - N_a, \quad (20)$$

where

$$N_a^0 = \sum_k c_{a,k}, \quad (21)$$

with $N_a = N_a^0$ due to Eq. (5), and $\mu_a = 1$ for each atom.

2.3.2 Functional derivative with respect to $\rho_a(\mathbf{r})$

Next, the functional derivative of L with respect to $\rho_a(\mathbf{r})$ is given by,²⁸

$$0 = \frac{\delta L}{\delta \rho_a(\mathbf{r})} = \ln \left(\frac{\rho_a(\mathbf{r})}{\rho_a^0(\mathbf{r})} \right) + \lambda(\mathbf{r}), \quad (22)$$

which leads to the stockholder partitioning formula,

$$\rho_a(\mathbf{r}) = \rho(\mathbf{r}) \frac{\rho_a^0(\mathbf{r})}{\rho^0(\mathbf{r})}. \quad (23)$$

2.3.3 Derivative with respect to $\alpha_{a,k}$

Now, consider the derivative of L with respect to $\alpha_{a,k}$,

$$0 = \frac{\partial L}{\partial \alpha_{a,k}} = \int_{\mathbb{R}^3} \frac{\delta L}{\delta \rho_a^0(\mathbf{r})} \frac{\partial \rho_a^0(\mathbf{r})}{\partial \alpha_{a,k}} d\mathbf{r} \quad (24)$$

$$= - \int_{\mathbb{R}^3} \frac{\rho_a(\mathbf{r})}{\rho_a^0(\mathbf{r})} \frac{\partial \rho_a^0(\mathbf{r})}{\partial \alpha_{a,k}} + \mu_a c_{a,k} \frac{\partial}{\partial \alpha_{a,k}} \int_{\mathbb{R}^3} g_{a,k}(\mathbf{r}) d\mathbf{r} \quad (25)$$

$$= \int_{\mathbb{R}^3} \frac{\rho_a(\mathbf{r})}{\rho_a^0(\mathbf{r})} \left(\frac{3}{n_{a,k} \alpha_{a,k}} - |\mathbf{r} - \mathbf{R}_a|^{n_{a,k}} \right) \rho_{a,k}^0(\mathbf{r}) d\mathbf{r}, \quad (26)$$

where Eq. (9) is used.

2.3.4 Derivative with respect to $n_{a,k}$

Finally, consider the derivative of L with respect to $n_{a,k}$,

$$0 = \frac{\partial L}{\partial n_{a,k}} = \int_{\mathbb{R}^3} \frac{\delta L}{\delta \rho_a^0(\mathbf{r})} \frac{\partial \rho_a^0(\mathbf{r})}{\partial n_{a,k}} d\mathbf{r} \quad (27)$$

$$= - \int_{\mathbb{R}^3} \frac{\rho_a(\mathbf{r})}{\rho_a^0(\mathbf{r})} \frac{\partial \rho_a^0(\mathbf{r})}{\partial n_{a,k}} + \mu_a c_{a,k} \frac{\partial}{\partial n_{a,k}} \int_{\mathbb{R}^3} g_{a,k}(\mathbf{r}) d\mathbf{r} \quad (28)$$

$$= \int_{\mathbb{R}^3} \frac{\rho_a(\mathbf{r})}{\rho_a^0(\mathbf{r})} \left(\frac{1}{n_{a,k}} - \frac{3 \ln(\alpha_{a,k})}{n_{a,k}^2} - \alpha_{a,k} |\mathbf{r} - \mathbf{R}_a|^{n_{a,k}} \ln(|\mathbf{r} - \mathbf{R}_a|) + \frac{3\psi(3/n_{a,k})}{n_{a,k}^2} \right) \rho_{a,k}^0(\mathbf{r}) d\mathbf{r} \quad (29)$$

with $\psi(z) = \frac{\Gamma'(z)}{\Gamma(z)}$, where Eq. (9) is also used.

2.3.5 Stationary points

The Lagrangian defined in Eq. (13) can therefore be simplified as

$$L[\{\rho_a\}, \{c_{a,k}\}, \{\alpha_{a,k}\}, \{n_{a,k}\}] = \sum_{a=1}^{N_{\text{atoms}}} \int_{\mathbb{R}^3} \rho_a(\mathbf{r}) \ln \left(\frac{\rho_a(\mathbf{r})}{\rho_a^0(\mathbf{r})} \right) d\mathbf{r} + \sum_{a=1}^{N_{\text{atoms}}} \left(\int_{\mathbb{R}^3} (\rho_a^0(\mathbf{r}) - \rho_a(\mathbf{r})) d\mathbf{r} \right), \quad (30)$$

such that it leads to exactly the same Euler–Lagrange Equations.

Indeed, the corresponding stationary points for $c_{a,k}$, $\alpha_{a,k}$, and $n_{a,k}$ are given by solving the following Euler-Lagrange equations,

$$c_{a,k} = \int_{\mathbb{R}^3} \frac{\rho_a(\mathbf{r})}{\rho_a^0(\mathbf{r})} \rho_{a,k}^0(\mathbf{r}) d\mathbf{r}, \quad (31)$$

$$\alpha_{a,k} = \frac{3c_{a,k}}{n_{a,k}} \left(\int_{\mathbb{R}^3} \frac{\rho_a(\mathbf{r})}{\rho_a^0(\mathbf{r})} \rho_{a,k}^0(\mathbf{r}) |\mathbf{r} - \mathbf{R}_a|^{n_{a,k}} d\mathbf{r} \right)^{-1}, \quad (32)$$

$$n_{a,k} = 3 \ln(\alpha_{a,k}) - 3\psi(3/n_{a,k}) + n_{a,k}^2 \alpha_{a,k} \int_{\mathbb{R}^3} \frac{\rho_a(\mathbf{r})}{\rho_a^0(\mathbf{r})} |\mathbf{r} - \mathbf{R}_a|^{n_{a,k}} \ln(|\mathbf{r} - \mathbf{R}_a|) g_{a,k}(\mathbf{r}) d\mathbf{r}, \quad (33)$$

in conjunction with Eq. (23).

2.4 ISA variants

A general solver for Eqs. (31)–(33) is the self-consistent method proposed in Ref. 28. In this section, different ISA variants are reproduced by fixing the variables defined in Eq. (13) using exponential basis functions as given in Eq. (10). More efficient solvers can then be employed depending on the corresponding variant.

The first variant is the nonlinear approximation of the ISA methods, referred to as NLIS,³⁰ in which $c_{a,k}$ and $\alpha_{a,k}$ are treated as variables, while $n_{a,k}$ is specified in advance as a hyperparameter. The reason $n_{a,k}$ is not treated as a variable is due to numerical difficulties, such as instabilities, that arise when solving Eq. (33), which involves the computation of higher-order moments.

When $n_{a,k} = 1$ is fixed and k corresponds to the number of subshells of the corresponding neutral atoms, the MBIS method is reproduced. A more generalized method compared to MBIS uses hyperparameters $n_{a,k}$, which are specified in advance. This method is referred to as the generalized MBIS method (GMBIS) in this work.

The self-consistent solver (SC) defined in Refs. 28,34 is employed in this work to solve the Euler-Lagrange equations for all nonlinear models, including NLIS, MBIS, and GMBIS. It should be noted that the solution to NLIS is generally not unique. However, with a good initial guess, a chemically reasonable solution can typically be obtained.²⁸

Furthermore, if both $n_{a,k}$ and $\alpha_{a,k}$ are fixed, i.e., only $c_{a,k}$ is treated as a variable, the linear approximation of the ISA method, denoted LISA, is reproduced.^{30,34} It should be noted that only exponential basis functions are considered in this work; in principle, any valid basis functions can be used. For example, one could also use the spherical average of atomic densities of atoms with partial charges, and the AVH method would be reproduced.³²

Different solvers can be applied in the LISA model, and based on whether $c_{a,k}$ is allowed to be negative, these solvers can be classified into two categories: **aLISA±** (allowing negative $c_{a,k}$) and **aLISA+** (using only non-negative $c_{a,k}$).³⁴ Different solvers within each category yield the same solutions because the optimization problem in the LISA model is convex. Therefore, we use SC and M-NEWTON as representatives of **aLISA+** and **aLISA±**, respectively. Further details can be found in Ref. 34.

2.5 Numerical computation

Analytically, solving the Euler-Lagrange equations derived from Eq. (30) is equivalent to solving those derived from an alternative Lagrangian:^{28,34}

$$L_{\text{glob}}[\{c_{a,k}\}, \{\alpha_{a,k}\}, \{n_{a,k}\}] = \int_{\mathbb{R}^3} \rho(\mathbf{r}) \ln \left(\frac{\rho(\mathbf{r})}{\rho^0(\mathbf{r})} \right) d\mathbf{r} + \int_{\mathbb{R}^3} (\rho^0(\mathbf{r}) - \rho(\mathbf{r})) d\mathbf{r}, \quad (34)$$

in conjunction with Eq. (30), where the AIM densities $\rho_a(\mathbf{r})$ are given as a set of the proatom densities $\rho_a^0(\mathbf{r})$. Note that Eq. (34) is independent of the AIM densities $\rho_a(\mathbf{r})$ and depends only on the molecular density. However, methods derived from Eq. (30) and Eq. (34) are generally not equivalent when using numerical quadrature, as the results depend on the grids used.

In principle, one can use both molecular grids and atomic grids for numerical integration. A molecular grid is constructed from a set of atomic grids, each defined as the tensor product of a radial grid and a spherical grid. Furthermore, nuclear weights, e.g., the Becke weight function ($w^B(\mathbf{r})$), are employed to avoid double-counting in grid points located in the overlap region of two atomic grids. The numerical version of Eq. (34) on a molecular grid can thus be written as:

$$\begin{aligned}
L_{\text{glob}}[\{c_{a,k}\}, \{\alpha_{a,k}\}, \{n_{a,k}\}] &= \sum_{i=1}^{N_{\text{pt}}^{\text{M}}} w^{\text{M}}(\mathbf{r}_i) \rho(\mathbf{r}_i) \ln \left(\frac{\rho(\mathbf{r}_i)}{\rho^0(\mathbf{r}_i)} \right) + \sum_{i=1}^{N_{\text{pt}}^{\text{M}}} w^{\text{M}}(\mathbf{r}_i) (\rho^0(\mathbf{r}_i) - \rho(\mathbf{r}_i)) \\
&= \sum_{a=1}^{N_{\text{atom}}} \sum_{j=1}^{N_{\text{pt}}^{\text{A}a}} w^{\text{A}a}(\mathbf{r}_{aj}) w^{\text{B}}(\mathbf{r}_{aj}) \rho(\mathbf{r}_{aj}) \ln \left(\frac{\rho(\mathbf{r}_{aj})}{\rho^0(\mathbf{r}_{aj})} \right) \\
&\quad + \sum_{a=1}^{N_{\text{atom}}} \sum_{j=1}^{N_{\text{pt}}^{\text{A}a}} w^{\text{A}a}(\mathbf{r}_{aj}) w^{\text{B}}(\mathbf{r}_{aj}) (\rho^0(\mathbf{r}_{aj}) - \rho(\mathbf{r}_{aj})), \tag{35}
\end{aligned}$$

with

$$w^{\text{M}}(\mathbf{r}_i) = w^{\text{A}a}(\mathbf{r}_{aj}) w^{\text{B}}(\mathbf{r}_{aj}), \tag{36}$$

$$N_{\text{pt}}^{\text{M}} = \sum_{a=1}^{N_{\text{atom}}} N_{\text{pt}}^{\text{A}a}, \tag{37}$$

where $w^{\text{M}}(\mathbf{r}_i)$ is the weight of the molecular grid at point i , $w^{\text{A}a}(\mathbf{r}_{aj})$ is the weight of the atomic grid Aa of atom a at point aj , and $w^{\text{B}}(\mathbf{r}_{aj})$ is the Becke weight at point aj . Here, the single index i is used for the molecular grid, while the double indices aj are used for atomic grids, with each i corresponding to a unique aj . N_{pt}^{M} denotes the number of molecular grid points, and $N_{\text{pt}}^{\text{A}a}$ represents the number of grid points in the atomic grid Aa of atom a .

Using atomic grids, the numerical version of Eq. (13) can be written as:

$$L[\{c_{a,k}\}, \{\alpha_{a,k}\}, \{n_{a,k}\}] = \sum_{a=1}^{N_{\text{atom}}} \sum_{j=1}^{N_{\text{pt}}^{Aa}} w^{Aa}(\mathbf{r}_{aj}) w_a(\mathbf{r}_{aj}) \rho(\mathbf{r}_{aj}) \ln \left(\frac{\rho(\mathbf{r}_{aj})}{\rho^0(\mathbf{r}_{aj})} \right) + \sum_{a=1}^{N_{\text{atom}}} \sum_{j=1}^{N_{\text{pt}}^{Aa}} w^{Aa}(\mathbf{r}_{aj}) w_a(\mathbf{r}_{aj}) (\rho^0(\mathbf{r}_{aj}) - \rho(\mathbf{r}_{aj})), \quad (38)$$

where $w_a(\mathbf{r}_{aj})$ is the AIM density weight of atom a at point aj . Since Eq. (38) is independent of the nuclear weights, we use Eq. (38) with only atomic grids, rather than the molecular grid, for all methods in this work. Therefore, the difference between Eq. (35) and Eq. (38) is to use the Becke weights or the Stockholder partitioning as partition of unity to localize the integrals.

2.6 Functionals and quantities of interest for ISA variants

In this section, several quantities of interest are introduced to assess the differences among the ISA variants. First, we decompose the atomic entropy defined in Eq. (1) into two components:

$$s_{\text{KL}}(\rho_a | \rho_a^0) = s_a^{\text{I+II}} = s_a^{\text{I}} + s_a^{\text{II}}, \quad (39)$$

where

$$s_a^{\text{I}} = s_{\text{KL}}(\rho_a | \langle \rho_a \rangle_s) = \int_{\mathbb{R}^3} \rho_a(\mathbf{r}) \ln \left(\frac{\rho_a(\mathbf{r})}{\langle \rho_a \rangle_s(r)} \right) d\mathbf{r}, \quad (40)$$

and

$$\begin{aligned} s_a^{\text{II}} &= s_{\text{KL}}(\langle \rho_a \rangle_s | \rho_a^0) = \int_{\mathbb{R}^3} \langle \rho_a \rangle_s(r) \ln \left(\frac{\langle \rho_a \rangle_s(r)}{\rho_a^0(r)} \right) d\mathbf{r} \\ &= 4\pi \int r^2 \langle \rho_a \rangle_s(r) \ln \left(\frac{\langle \rho_a \rangle_s(r)}{\rho_a^0(r)} \right) dr, \end{aligned} \quad (41)$$

with the spherical average of the atomic density $\langle \rho_a \rangle_s(r)$ defined as:

$$\langle \rho_a \rangle_s(r) = \frac{1}{4\pi} \int_0^\pi \sin(\theta) \int_0^{2\pi} \rho_a(\mathbf{r}) d\theta d\phi. \quad (42)$$

Here, s_a^{I} corresponds to the entropy arising from the anisotropy of the AIM density of atom a in the molecule. If the atomic density is spherically symmetric, s_a^{I} is zero; otherwise, it is nonzero. On the other hand, s_a^{II} represents the entropy due to the completeness of the basis functions used to construct the proatom density of atom a . In the complete basis set limit, there holds $s_a^{\text{II}} = 0$.

We also introduce two quantities:

$$n_a(r) = 4\pi r^2 \langle \rho_a \rangle_s(r), \quad (43)$$

$$s_a(r) = 4\pi r^2 \langle \rho_a \rangle_s(r) \ln \left(\frac{\langle \rho_a \rangle_s(r)}{\rho_a^0(r)} \right), \quad (44)$$

where $n_a(r)dr$ represents the contribution to the atomic population of atom a in the interval $[r, r + dr]$.²⁴ Similarly, $s_a(r)dr$ represents the contribution to the atomic entropy of atom a in the interval $[r, r + dr]$, revealing discrepancies between $\langle \rho_a \rangle_s(r)$ and $\rho_a^0(r)$.

Furthermore, we introduce the absolute Kullback–Leibler entropy, denoted as t_{KL} . The corresponding atomic absolute Kullback–Leibler entropy, t_a , is then defined to describe the deviation between $\rho_a(\mathbf{r})$ and $\rho_a^0(\mathbf{r})$, following the conventions in Eq. (2):

$$t_a = t_{\text{KL}}(\rho_a | \rho_a^0) = \int_{\mathbb{R}^3} \rho_a(\mathbf{r}) \left| \ln \left(\frac{\rho_a(\mathbf{r})}{\rho_a^0(\mathbf{r})} \right) \right| d\mathbf{r}, \quad (45)$$

and the molecular absolute Kullback–Leibler entropy of a molecule is then defined as

$$T = \sum_a t_a. \quad (46)$$

3 Computational details

As introduced in Section 2, the implementation of the ISA method and its variants requires numerical quadrature, with atomic grids employed. Each atomic grid consists of radial and angular components. For simplicity, 150 Gauss-Chebyshev radial points and 194 Lebedev-Laikov angular points were used for all atoms. The Gauss-Chebyshev integration interval $[-1, 1]$ was mapped to the semi-infinite radial interval $[0, +\infty)$, following Ref. 35.

All calculations were performed using the Horton-Part 1.1.6 package.³⁶ on a MacBook Pro equipped with an Apple M2 Pro chip featuring 12 cores (8 performance cores and 4 efficiency cores) and 16 GB of memory. The input files were prepared using the Horton 3 package.³⁷⁻⁴⁰ The IOData⁴¹ and GBasis³⁸ packages were used to prepare the molecular density and its gradients on grid points generated by the Grid package.³⁹

For benchmarking, five molecules (CCl_4 , CS_2 , CH_4 , NH_3 , H_2O) and six charged molecular ions (CH_3^+ , CH_3^- , NH_4^+ , NH_2^- , H_3O^+ , OH^-) were taken from Ref. 34. Molecular structures were optimized using DFT at the B3LYP/aug-cc-pVDZ level of theory. Molecular density calculations were performed at the LDA/aug-cc-pVDZ level of theory,^{42,43} which showed good agreement with experimental data from previous studies.¹⁹

Additionally, four boron wheel molecules were included: B_8 , B_8^{2-} , B_8 triplet, and B_9^- . The structures of B_8 , B_8 triplet, and B_8^{2-} are perfect heptagons, while B_9^- forms a perfect octagon. These structures were obtained from Ref. 44. Molecular density calculations for the boron wheels were performed at the PBE/6-31+G(d,p) level of theory. The optimized coordinates of all test molecules are provided in Tables S1–S15 in Section S1 in the Supporting Information.

In addition, isolated atomic densities were computed for constructing the basis functions used in the LISA and GMBIS models. Table 1 lists the isolated atomic densities calculated at the PBE/6-311+G(d,p) level of theory. For hydrogen, atomic densities with charges of 0, -1, and -2 were computed. For lithium, atomic densities with charges of +2, +1, 0, -1, and -2 were computed. For

boron, carbon, nitrogen, oxygen, fluorine, silicon, sulfur, chlorine, and bromine, atomic densities with charges of +3, +2, +1, 0, -1, and -2 were computed. All DFT calculations were performed using the GAUSSIAN16 package.⁴⁵ Input files for the atomic density calculations were generated using the Horton 3 package.³⁷

Table 1: Atomic data with various charges employed in this work for fitting hyperparameters of the GMBIS model.

| Atom | Charges |
|------------------------------|-----------------------|
| H | 0, -1, -2 |
| Li | +2, +1, 0, -1, -2 |
| B, C, N, O, F, Si, S, Cl, Br | +3, +2, +1, 0, -1, -2 |

ISA and several its variants were considered in this work, including six LISA models, four NLIS models, and two special NLIS models: MBIS and GMBIS. The first LISA model, referred to as LISA1, is the LISA model with Gaussian basis functions, as defined in Ref. 34 employing the SC solver. The second LISA model, denoted by LISA2, corresponds to the LISA model with Gaussian basis functions and an additional Slater function for hydrogen, as defined in Ref. 34, also using the SC solver. Only results for molecules containing hydrogen thus differ between LISA1 and LISA2.

The MBIS model²⁸ was used with convergence criteria set to match those of LISA1 and LISA2, as described in Ref. 34. The order n_{ak} for the GMBIS model for each element was optimized using the NLIS model, with the same k for each element as in MBIS. The spherical averages of isolated atomic densities with various charges, as listed in Table 1, were fitted using NLIS by selecting a set of hyperparameters n_{ak} . The final hyperparameters n_{ak} were determined by minimizing the sum of all entropies for each element. For instance for hydrogen n_{ak} , the coefficients are obtained by

$$\min \left\{ \sum_{q=-2}^0 s_{\text{KL}}(\rho_q | \rho_q^0) \right\} = \min \left\{ \sum_{q=-2}^0 \int_{\mathbb{R}^+} \langle \rho_q \rangle_s(r) \ln \left(\frac{\langle \rho_q \rangle_s(r)}{\rho_q^0(r)} \right) \right\}, \quad (47)$$

where $\langle \rho_q \rangle_s(r)$ and $\rho_q(r)$ correspond to the spherical average of the atomic density and the NLIS

pro-atom density of the hydrogen atom with different charges q , respectively. The final values of n_{ak} for each shell k of each element are presented in Table 2.

Table 2: Optimized n_{ak} values for each element used in the GMBIS model.

| Atom | $k = 1$ | $k = 2$ | $k = 3$ |
|-------------|---------|---------|---------|
| H | 1.038 | -- | -- |
| Li | 1.000 | 1.069 | -- |
| B | 1.069 | 1.000 | -- |
| C | 1.138 | 1.000 | -- |
| N | 1.172 | 1.000 | -- |
| O | 1.172 | 1.000 | -- |
| F | 1.138 | 1.000 | -- |
| Si | 1.111 | 1.667 | 1.000 |
| S | 1.000 | 2.000 | 1.000 |
| Cl | 1.111 | 2.000 | 1.000 |
| Br | 1.111 | 2.000 | 1.000 |

The first general NLIS model, denoted NLIS1, uses the same number of basis functions as LISA1, with Gaussian functions ($n_{a,k} = 2$) for all basis functions of an atom. The optimized results of the NLIS model depend on the initial values.^{28,30} In this work, the initial values for $c_{a,k}$ in all generalized NLIS models were set to Z/N_k , where Z is the atomic number of atom a and N_k is the number of basis functions. The initial values for $\alpha_{a,k}$ were set to those used in the MBIS model, except for the outermost shell of an atom, where a value of 0.5 was used instead of 2, as in the MBIS model.²⁸ The SC solver, described in Ref. 28, was used for all NLIS models. The second NLIS model, denoted NLIS2, was defined similarly to NLIS1, except that one Gaussian function was replaced by a Slater function for each element. The third NLIS model (NLIS3) extends NLIS2 by replacing an additional Gaussian basis function with a Slater function for each atom. The final generalized NLIS model (NLIS4) uses only Slater basis functions, with $n_{a,k} = 1$ for all atoms. The same initial values as in NLIS1 were used.

The third LISA model (LISA3) uses Gaussian basis functions fitted using the NLIS1 model. Specifically, the NLIS1 model was applied to isolated atoms with various charges. Data for atoms

with charges of +2, +1, 0, -1, and -2 were considered, while for hydrogen, only charges of 0, -1, and -2 were used. The optimized $\alpha_{a,k}$ and $c_{a,k}$ values were collected to form a new basis set for fitting molecular densities. Functions with $c_{a,k}$ values smaller than 10^{-4} were removed. Two functions were combined into one if $\frac{\alpha_1 - \alpha_2}{\alpha_1 + \alpha_2} < 0.1$, with the new α calculated as the average of α_1 and α_2 . The new $c_{a,k}$ was set as the sum of the $c_{a,k}$ values from the two functions. The M-NEWTON solver was used.³⁴ The fourth LISA model (LISA4) is based on LISA3, except that the SC solver was used.³⁴ The fifth LISA model (LISA5) is similar to LISA3 but uses the NLIS4 model to fit atomic densities. The final LISA model (LISA6) is the same as LISA5, except that the SC solver was used.³⁴

Table 3 summarizes all methods used in this work. An alternating iteration scheme, as described in Ref. 34, was applied to all methods. The criterion for the outer iteration, set to 10^{-8} , follows the approach in Ref. 34, while the criterion for the inner iteration was set to 10^{-9} .

Table 3: Definitions of all methods used in this work.

| Model | Description |
|--------------|---|
| ISA | The ISA model, as defined in Ref. 21,22. |
| LISA1 | The LISA model with Gaussian basis functions, as defined in Ref. 34, using the SC solver. |
| LISA2 | The LISA1 model with an additional Slater function for hydrogen, as defined in Ref. 34. |
| MBIS | The MBIS model, as defined in Ref. 34, using the SC solver. |
| NLIS1 | The NLIS model with the same number of basis functions as LISA1, using Gaussian functions ($n_{a,k} = 2$) for all basis functions, and the SC solver. |
| NLIS2 | The NLIS1 model with one Gaussian function replaced by a Slater function for each element. |

Continued on next page

Table 3: (continued)

| Model | Description |
|-------|---|
| NLIS3 | The NLIS1 model with two Gaussian basis functions replaced by Slater functions for each atom. |
| NLIS4 | The NLIS1 model using only Slater basis functions ($n_{a,k} = 1$) for all atoms. |
| LISA3 | The LISA model combined with Gaussian basis functions obtained by fitting atomic data using the NLIS1 model. The M-NEWTON solver is used. ³⁴ |
| LISA4 | Same as LISA3, except that the SC solver is used. ³⁴ |
| LISA5 | Same as LISA3, except that the NLIS4 model is used to obtain the basis functions by fitting atomic data. |
| LISA6 | Same as LISA5, except that the SC solver is used. ³⁴ |
| GMBIS | The order n_{ak} for each atom is optimized using the NLIS model, with the same k as in MBIS. |

4 Results

The optimized $n_{a,k}$, $\alpha_{a,k}$, and $c_{a,k}$ parameters for all test molecules across all methods are provided in Tables S16–S30 in Section S2 of the Supporting Information. Partitioning results, including S , T , and other quantities of interest for each atom in each molecule, are presented in Tables S31–S45 in Section S3 of the Supporting Information. Comparisons of radial densities $\rho_a^0(r)$ with $\langle \rho_a \rangle_s(r)$, as well as $\rho_a(r)$ with entropy $s_a(r)$ for atom a in all test molecules across the NLIS1, LISA4, MBIS, and ISA methods, are shown in Figs. S1–S45 in Section S4 of the Supporting Information.

The comparison of T and S for all test molecules across different methods is presented in Figure 1. Methods with lower S generally exhibit lower T , although exceptions exist, as listed in Table S46 of the Supporting Information. Figure 2 presents $\log_{10}(S/n_{\text{atom}})$ values for each

molecule, where n_{atom} is the number of atoms in the molecule. The corresponding $\log_{10}(T/n_{\text{atom}})$ values are shown in Fig. 3. Results for LISA3 and LISA5 are unavailable for most molecules due to the large number of basis functions used, which often cause invalid line searches in the M-NEWTON solver.³⁴

Additionally, Figure 4 provides $\log_{10}(s_a^{\text{I}})$ values for atom a in each molecule using different methods. For molecules without boron atoms, a represents C, N, or O atoms, while for boron wheel molecules, a refers to the central B atom. Figures 5 and 6 are analogous to Figure 4, showing $\log_{10}(s_a^{\text{II}})$ and q_a values, respectively.

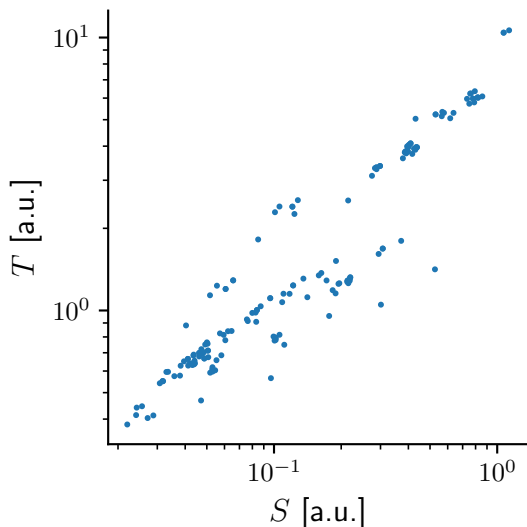


Figure 1: Comparison of T and S (in a.u.) for all test molecules across different methods.

NLIS1 consistently achieves the lowest S and T values, with some exceptions. For example, in CH_3^- , LISA3 yields a lower S than NLIS1, while NLIS1 provides a lower T than LISA3, as detailed in Table S46. The ordering of S and T for the NLIS models is $\text{NLIS1} < \text{NLIS2} < \text{NLIS3} < \text{NLIS4} \leq \text{MBIS}$, where $<$ (\leq) indicates that the method on the left produces a lower (or not higher) value than the method on the right.

Lower S and T values generally correspond to better numerical performance in fitting atomic densities. GMBIS produces S values not greater than MBIS, though the differences are minor.

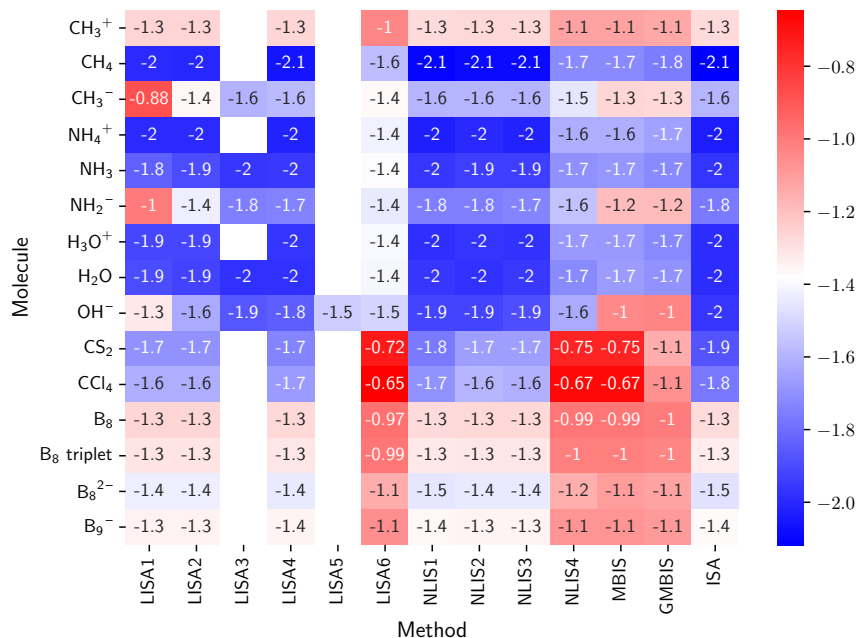


Figure 2: $\log_{10}(S/n_{\text{atom}})$ values for each molecule using various methods, where n_{atom} is the number of atoms in the molecule.

However, GMBIS does not fully address issues associated with MBIS, such as overly negative atomic charges in anionic molecules like CH_3^- and NH_3^- , as shown in Fig. 6. Delocalized systems exhibit substantial differences in atomic charges between MBIS or GMBIS and NLIS models. For instance, the central B atom charge in B_8 is 0.37 for NLIS1, NLIS2, and NLIS3, compared to 0.11 and 0.12 for MBIS and GMBIS, respectively. Fig. 7 compares NLIS1 with MBIS, LISA4, and ISA methods for the central B atom in B_8 . The left panels show $\rho_a^0(r)$ and $\langle \rho_a \rangle_s(r)$, while the right panels display $s_a(r)$ and $n_a(r)$. In the comparison with MBIS, NLIS1 shows smoother decay in $\rho_a^0(r)$ and $\langle \rho_a \rangle_s(r)$, with fewer oscillations in $s_a(r)$, leading to a lower s_a^{II} value. The comparisons with LISA4 and ISA indicate that NLIS1 provides more consistent and physically meaningful partitioning, with LISA4 closely matching NLIS1.

For most molecules, NLIS4 and MBIS yield similar S and T values, and the number of unique exponents $\alpha_{a,k}$ obtained by NLIS4 matches the number of basis functions used in MBIS, as shown in the Supporting Information. This suggests that simply adding more basis functions does not

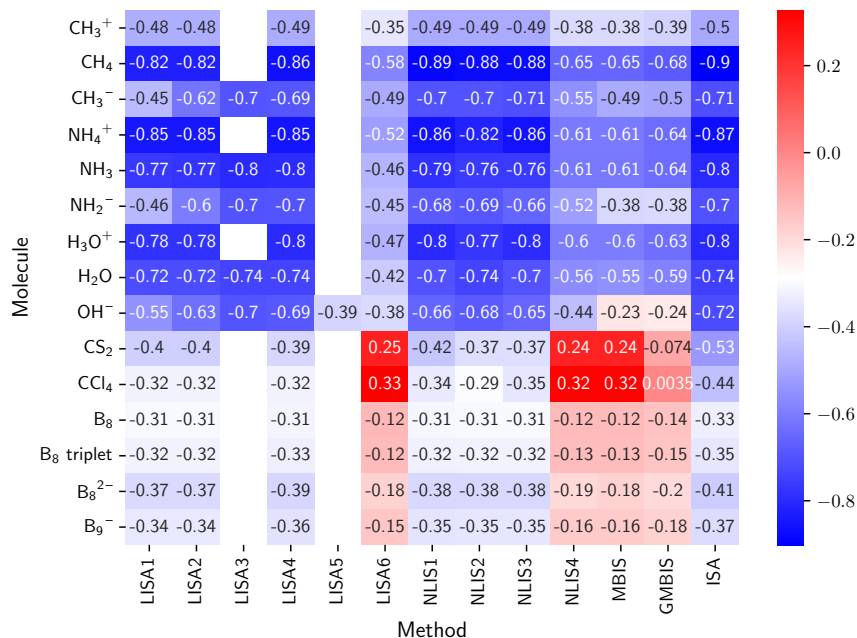


Figure 3: $\log_{10}(T/n_{\text{atom}})$ values for each molecule using various methods, where n_{atom} is the number of atoms in the molecule.

trivially improve MBIS results. Additionally, LISA6 yields higher S values compared to MBIS in certain molecular systems, as shown in Figure 2, despite using more Slater basis functions than MBIS.

For the LISA methods, the ordering is (LISA3 \leq) LISA4 < LISA2 \leq LISA1 < (LISA5 \leq) LISA6, with parentheses indicating cases where the method converged. The S and T values for LISA4 closely align with NLIS1, demonstrating that Gaussian basis functions used in LISA4 are robust and generalizable.

Both LISA1 and LISA2 yield similar S values to NLIS1, LISA4, or ISA, except for CH₃⁻, NH₂⁻, and OH⁻, where LISA2 achieves a lower S than LISA1 by including an additional Slater function for hydrogen.³⁴ However, differences in atomic charges for C, N, and O atoms persist between LISA2 and LISA4 (or NLIS1 or ISA) for these molecules. Adding an extra Slater function to hydrogen significantly reduces s_{C}^{I} in CH₃⁻ compared to MBIS, as shown in Figure 4. Nevertheless, this approach may still produce less reliable results than LISA4 or NLIS1 in chemical

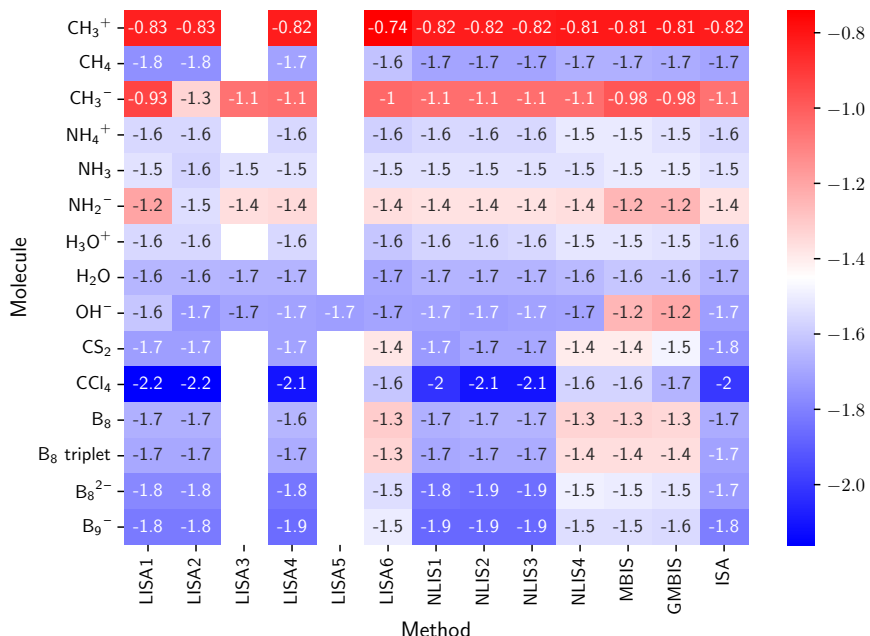


Figure 4: $\log_{10}(s_a^I)$ values for atom a in each molecule, calculated using different methods. For molecules without a boron atom, a represents C, N, or O atoms, while for molecules containing a boron atom, a refers to the central B atom.

applications.

The s_a^I values for selected atoms, shown in Fig. 4, indicate that LISA4, NLIS1, and NLIS2 align closely with ISA. These methods yield similar atomic charges, as depicted in Fig. 6. Notably, when MBIS and GMBIS predict s_a^I values close to those from LISA4, NLIS1, and ISA, the corresponding atomic charges are also similar. However, for certain molecules, such as CH₃⁻, OH⁻, NH₂⁻, CS₂, CCl₄, and the boron wheel molecules, MBIS and GMBIS produce significantly different s_a^I values. In these cases, the atomic charges predicted by MBIS and GMBIS deviate substantially from those obtained by LISA4 or NLIS1.

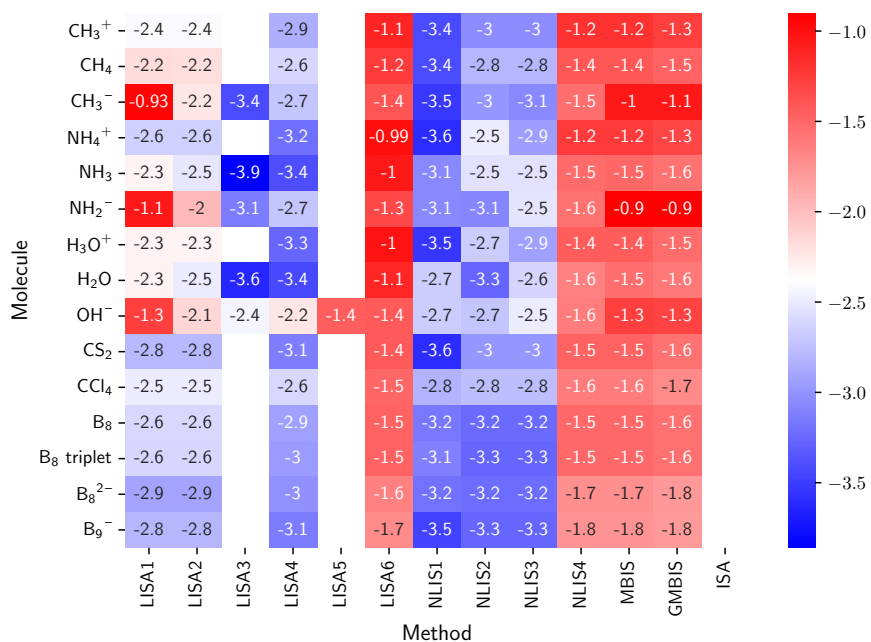


Figure 5: Same as Fig. 4, but for $\log_{10}(s_a^{\text{II}})$ values.

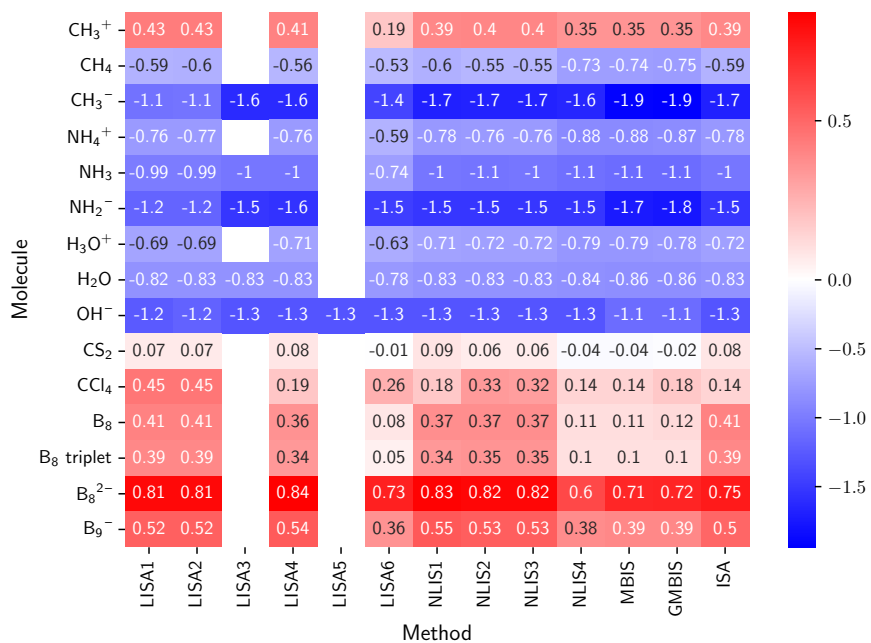


Figure 6: Same as Fig. 4, but for atomic charges q_a .

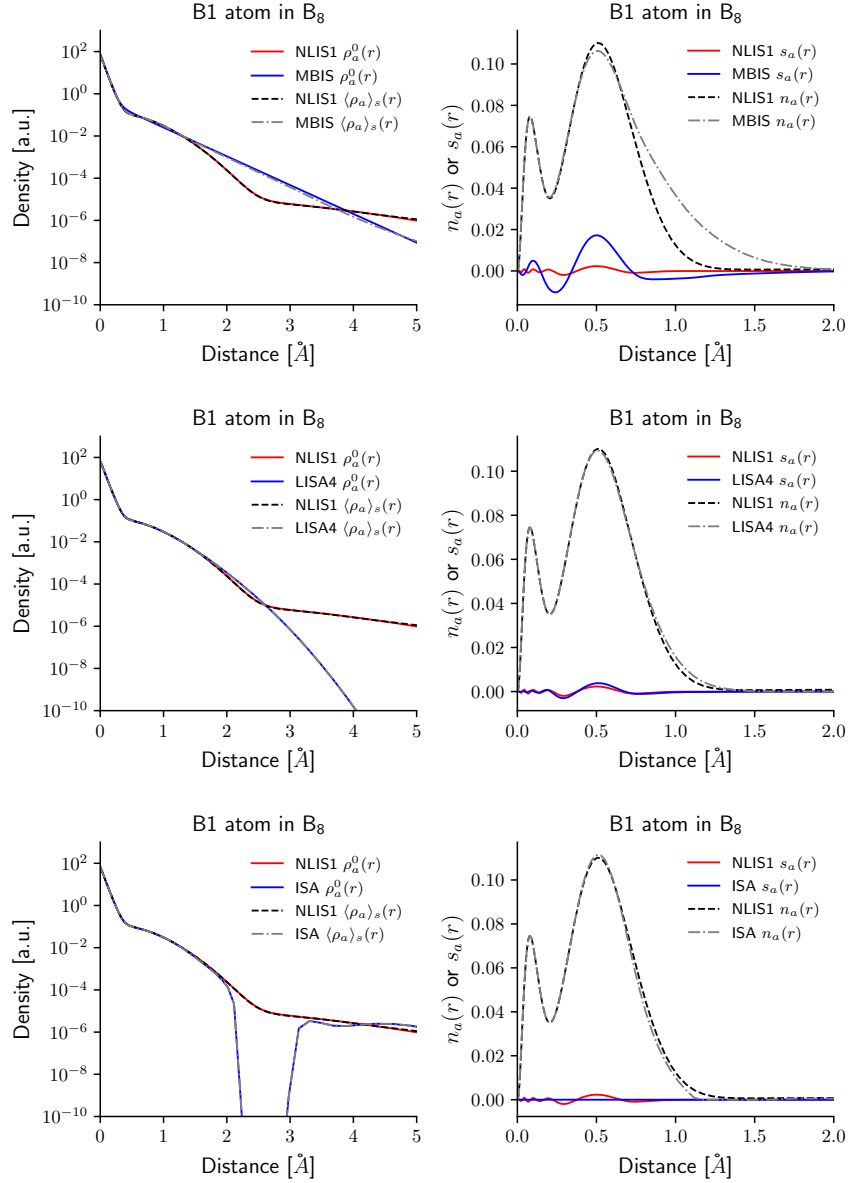


Figure 7: Comparison of quantities between NLIS1 and other methods, including MBIS, LISA4, and ISA, for the central B atom in B₈. The left panels show $\rho_a^0(r)$ and $\langle \rho_a \rangle_s(r)$, while the right panels display $s_a(r)$ and $n_a(r)$.

5 Summary

This study investigates linear and non-linear approximations of ISA partitioning methods, denoted as LISA and NLIS, respectively, employing exponential basis functions as an alternative to the pointwise discretization used in the original ISA method. A general NLIS model is formulated using a generalized Lagrangian framework with exponential basis functions, treating both the exponential order and degree as variables. However, due to numerical difficulties, the degree of exponential functions is treated as a hyperparameter in all NLIS models. The well-established MBIS model is reproduced by using only Slater-type basis functions with the number of basis functions fixed for each element. A generalized MBIS model is developed by optimizing the degree of exponential basis functions for each element type independently, relaxing the constraint of using pure Slater-type forms.

LISA models are reproduced by fixing the exponents and degrees of the basis functions, and a set of LISA variants is proposed. The LISA4 model employs Gaussian basis functions, with exponents optimized by fitting atomic densities using the NLIS model. All computations were performed using the open-source *Horton-Part* program and benchmarked on molecules and charged ions, including four boron wheel molecules with significantly delocalized bonding environments.

To evaluate model performance, several partitioning metrics are introduced, including absolute entropy and the radial distribution of atomic entropy. Among the methods tested, NLIS1, which exclusively uses Gaussian-type basis functions, achieved the lowest molecular entropy values and excelled in other metrics. The results for the LISA4 model closely align with those of NLIS1 across all metrics. Both LISA4 and NLIS1 show strong agreement with the ISA method, particularly in terms of atomic charges.

In summary, this work addresses the well-known issue in ISA partitioning by employing basis function approaches in all proposed models. Considering computational efficiency, numerical stability, and accuracy, LISA4 is identified as the recommended model.

Acknowledgement

Y.C. and B.S. acknowledge funding by the Deutsche Forschungsgemeinschaft (DFG, German Research Foundation) - Project number 442047500 through the Collaborative Research Center “Sparsity and Singular Structures” (SFB 1481). We also thank the Deutsche Forschungsgemeinschaft (DFG, German Research Foundation) for supporting this work by funding - EXC2075 – 390740016 under Germany’s Excellence Strategy. We acknowledge the support by the Stuttgart Center for Simulation Science (SimTech). The resources and services used in this work were provided by the VSC (Flemish Supercomputer Center), funded by the Research Foundation - Flanders (FWO) and the Flemish Government.

References

- (1) Warshel, A.; Levitt, M. Theoretical Studies of Enzymic Reactions: Dielectric, Electrostatic and Steric Stabilization of the Carbonium Ion in the Reaction of Lysozyme. *J. Mol. Biol.* **1976**, *103*, 227–249.
- (2) Kaminski, G. A.; Stern, H. A.; Berne, B. J.; Friesner, R. A.; Cao, Y. X.; Murphy, R. B.; Zhou, R.; Halgren, T. A. Development of a Polarizable Force Field for Proteins via Ab Initio Quantum Chemistry: First Generation Model and Gas Phase Tests. *J. Comput. Chem.* **2002**, *23*, 1515–1531.
- (3) Ren, P.; Ponder, J. W. Consistent Treatment of Inter- and Intramolecular Polarization in Molecular Mechanics Calculations. *J. Comput. Chem.* **2002**, *23*, 1497–1506.
- (4) Jorgensen, W. L.; Jensen, K. P.; Alexandrova, A. N. Polarization Effects for Hydrogen-Bonded Complexes of Substituted Phenols with Water and Chloride Ion. *J. Chem. Theory Comput.* **2007**, *3*, 1987–1992.

- (5) Shi, Y.; Xia, Z.; Zhang, J.; Best, R.; Wu, C.; Ponder, J. W.; Ren, P. Polarizable Atomic Multipole-Based AMOEBA Force Field for Proteins. *J. Chem. Theory Comput.* **2013**, *9*, 4046–4063.
- (6) Lamoureux, G.; Roux, B. Modeling Induced Polarization with Classical Drude Oscillators: Theory and Molecular Dynamics Simulation Algorithm. *J. Chem. Phys.* **2003**, *119*, 3025–3039.
- (7) Yu, H.; Hansson, T.; van Gunsteren, W. F. Development of a Simple, Self-Consistent Polarizable Model for Liquid Water. *J. Chem. Phys.* **2003**, *118*, 221–234.
- (8) Lemkul, J. A.; Huang, J.; Roux, B.; MacKerell, A. D. J. An Empirical Polarizable Force Field Based on the Classical Drude Oscillator Model: Development History and Recent Applications. *Chem. Rev.* **2016**, *116*, 4983–5013.
- (9) Kunz, A.-P. E.; van Gunsteren, W. F. Development of a Nonlinear Classical Polarization Model for Liquid Water and Aqueous Solutions: COS/D. *J. Phys. Chem. A* **2009**, *113*, 11570–11579.
- (10) Mortier, W. J.; Van Genechten, K.; Gasteiger, J. Electronegativity Equalization: Application and Parametrization. *J. Am. Chem. Soc.* **1985**, *107*, 829–835.
- (11) Mortier, W. J.; Ghosh, S. K.; Shankar, S. Electronegativity-Equalization Method for the Calculation of Atomic Charges in Molecules. *J. Am. Chem. Soc.* **1986**, *108*, 4315–4320.
- (12) Kale, S.; Herzfeld, J. Pairwise Long-Range Compensation for Strongly Ionic Systems. *J. Chem. Theory Comput.* **2011**, *7*, 3620–3624.
- (13) Kale, S.; Herzfeld, J.; Dai, S.; Blank, M. Lewis-Inspired Representation of Dissociable Water in Clusters and Grothuss Chains. *J. Biol. Phys.* **2012**, *38*, 49–59.

- (14) Kale, S.; Herzfeld, J. Natural Polarizability and Flexibility via Explicit Valency: The Case of Water. *J. Chem. Phys.* **2012**, *136*, 084109.
- (15) Bai, C.; Kale, S.; Herzfeld, J. Chemistry with Semi-Classical Electrons: Reaction Trajectories Auto-Generated by Sub-Atomistic Force Fields. *Chem. Sci.* **2017**, *8*, 4203–4210.
- (16) Cools-Ceuppens, M.; Dambre, J.; Verstraelen, T. Modeling Electronic Response Properties with an Explicit-Electron Machine Learning Potential. *J. Chem. Theory Comput.* **2022**, *18*, 1672–1691.
- (17) Verstraelen, T.; Ayers, P. W.; Van Speybroeck, V.; Waroquier, M. ACKS2: Atom-condensed Kohn-Sham DFT Approximated to Second Order. *J. Chem. Phys.* **2013**, *138*, 074108.
- (18) Verstraelen, T.; Vandenbrande, S.; Ayers, P. W. Direct Computation of Parameters for Accurate Polarizable Force Fields. *J. Chem. Phys.* **2014**, *141*, 194114.
- (19) Cheng, Y.; Verstraelen, T. A new framework for frequency-dependent polarizable force fields. *J. Chem. Phys.* **2022**, *157*, 124106.
- (20) Ayers, P. W. Atoms in molecules, an axiomatic approach. I. Maximum transferability. *J. Chem. Phys.* **2000**, *113*, 10886–10898.
- (21) C. Lillestolen, T.; J. Wheatley, R. Redefining the atom: atomic charge densities produced by an iterative stockholder approach. *Chem. Commun.* **2008**, *0*, 5909–5911.
- (22) Lillestolen, T. C.; Wheatley, R. J. Atomic charge densities generated using an iterative stockholder procedure. *J. Chem. Phys.* **2009**, *131*, 144101.
- (23) Bultinck, P.; L. Cooper, D.; Neck, D. V. Comparison of the Hirshfeld-I and iterated stockholder atoms in molecules schemes. *Phys. Chem. Chem. Phys.* **2009**, *11*, 3424–3429.

- (24) Verstraelen, T.; Ayers, P. W.; Van Speybroeck, V.; Waroquier, M. The Conformational Sensitivity of Iterative Stockholder Partitioning Schemes. *Chem. Phys. Lett.* **2012**, *545*, 138–143.
- (25) Verstraelen, T.; Ayers, P. W.; Van Speybroeck, V.; Waroquier, M. Hirshfeld-E Partitioning: AIM Charges with an Improved Trade-off between Robustness and Accurate Electrostatics. *J. Chem. Theory Comput.* **2013**, *9*, 2221–2225.
- (26) Misquitta, A. J.; Stone, A. J.; Fazeli, F. Distributed Multipoles from a Robust Basis-Space Implementation of the Iterated Stockholder Atoms Procedure. *J. Chem. Theory Comput.* **2014**, *10*, 5405–5418.
- (27) Heidar-Zadeh, F.; Ayers, P. W. How pervasive is the Hirshfeld partitioning? *J. Chem. Phys.* **2015**, *142*, 044107.
- (28) Verstraelen, T.; Vandenbrande, S.; Heidar-Zadeh, F.; Vanduyfhuys, L.; Van Speybroeck, V.; Waroquier, M.; Ayers, P. W. Minimal Basis Iterative Stockholder: Atoms in Molecules for Force-Field Development. *J. Chem. Theory Comput.* **2016**, *12*, 3894–3912.
- (29) Heidar-Zadeh, F.; Ayers, P. W.; Verstraelen, T.; Vinogradov, I.; Vöhringer-Martinez, E.; Bultinck, P. Information-Theoretic Approaches to Atoms-in-Molecules: Hirshfeld Family of Partitioning Schemes. *J. Phys. Chem. A* **2018**, *122*, 4219–4245.
- (30) Benda, R.; Cancès, E.; Ehrlacher, V.; Stamm, B. Multi-Center Decomposition of Molecular Densities: A Mathematical Perspective. *J. Chem. Phys.* **2022**, *156*, 164107.
- (31) Heidar-Zadeh, F. Variational Information-Theoretic Atoms-in-Molecules. Thesis, 2017; Accepted: 2017-10-03T19:42:29Z.
- (32) Heidar-Zadeh, F.; Castillo-Orellana, C.; van Zyl, M.; Pujal, L.; Verstraelen, T.; Bultinck, P.; Vöhringer-Martinez, E.; Ayers, P. W. Variational Hirshfeld Partitioning: General Framework

- and the Additive Variational Hirshfeld Partitioning Method. *Journal of Chemical Theory and Computation* **2024**, *XX*, XX–XX, Publisher: American Chemical Society.
- (33) Parr, R. G.; Ayers, P. W.; Nalewajski, R. F. What Is an Atom in a Molecule? *J. Phys. Chem. A* **2005**, *109*, 3957–3959.
- (34) Cheng, Y.; Cancès, E.; Ehlacher, V.; Misquitta, A. J.; Stamm, B. Multi-center decomposition of molecular densities: A numerical perspective. 2024; <http://arxiv.org/abs/2405.08455>, arXiv:2405.08455 [physics].
- (35) Becke, A. D. A multicenter numerical integration scheme for polyatomic molecules. *J. Chem. Phys.* **1988**, *88*, 2547–2553.
- (36) Cheng, Y. Horton-Part 1.1.5. 2024; <https://github.com/LISA-partitioning-method/horton-part>, Accessed on Oct 02, 2024.
- (37) Chan, M.; Verstraelen, T.; Tehrani, A.; Richer, M.; Yang, X. D.; Kim, T. D.; Vöhringer-Martinez, E.; Heidar-Zadeh, F.; Ayers, P. W. The tale of HORTON: Lessons learned in a decade of scientific software development. *J. Chem. Phys.* **2024**, *160*, 162501.
- (38) Kim, T. D.; Pujal, L.; Richer, M.; van Zyl, M.; Martínez-González, M.; Tehrani, A.; Chuiko, V.; Sánchez-Díaz, G.; Sanchez, W.; Adams, W.; Huang, X.; Kelly, B. D.; Vöhringer-Martinez, E.; Verstraelen, T.; Heidar-Zadeh, F.; Ayers, P. W. GBasis: A Python library for evaluating functions, functionals, and integrals expressed with Gaussian basis functions. *J. Chem. Phys.* **2024**, *161*, 042503.
- (39) Tehrani, A.; Yang, X. D.; Martínez-González, M.; Pujal, L.; Hernández-Esparza, R.; Chan, M.; Vöhringer-Martinez, E.; Verstraelen, T.; Ayers, P. W.; Heidar-Zadeh, F. Grid: A Python library for molecular integration, interpolation, differentiation, and more. *J. Chem. Phys.* **2024**, *160*, 172503.

- (40) theochem/denspart. 2024; <https://github.com/theochem/denspart>, Accessed on Apr 08, 2024.
- (41) Verstraelen, T.; Adams, W.; Pujal, L.; Tehrani, A.; Kelly, B. D.; Macaya, L.; Meng, F.; Richer, M.; Hernández-Esparza, R.; Yang, X. D.; Chan, M.; Kim, T. D.; Cools-Ceuppens, M.; Chuiko, V.; Vöhringer-Martinez, E.; Ayers, P. W.; Heidar-Zadeh, F. IOData: A python library for reading, writing, and converting computational chemistry file formats and generating input files. *J. Comput. Chem.* **2021**, *42*, 458–464.
- (42) Kohn, W.; Sham, L. J. Self-Consistent Equations Including Exchange and Correlation Effects. *Phys. Rev.* **1965**, *140*, A1133–A1138.
- (43) Kendall, R. A.; Dunning, T. H.; Harrison, R. J. Electron affinities of the first-row atoms revisited. Systematic basis sets and wave functions. *J. Chem. Phys.* **1992**, *96*, 6796–6806.
- (44) Zhai, H.-J.; Alexandrova, A. N.; Birch, K. A.; Boldyrev, A. I.; Wang, L.-S. Hepta- and Octa-coordinate Boron in Molecular Wheels of Eight- and Nine-Atom Boron Clusters: Observation and Confirmation. *Angewandte Chemie International Edition* **2003**, *42*, 6004–6008.
- (45) Frisch, M. J.; Trucks, G. W.; Schlegel, H. B.; Scuseria, G. E.; Robb, M. A.; Cheeseman, J. R.; Scalmani, G.; Barone, V.; Petersson, G. A.; Nakatsuji, H.; Li, X.; Caricato, M.; Marenich, A. V.; Bloino, J.; Janesko, B. G.; Gomperts, R.; Mennucci, B.; Hratchian, H. P.; Ortiz, J. V.; Izmaylov, A. F.; Sonnenberg, J. L.; Williams-Young, D.; Ding, F.; Lipparini, F.; Egidi, F.; Goings, J.; Peng, B.; Petrone, A.; Henderson, T.; Ranasinghe, D.; Zakrzewski, V. G.; Gao, J.; Rega, N.; Zheng, G.; Liang, W.; Hada, M.; Ehara, M.; Toyota, K.; Fukuda, R.; Hasegawa, J.; Ishida, M.; Nakajima, T.; Honda, Y.; Kitao, O.; Nakai, H.; Vreven, T.; Throssell, K.; Montgomery, J. A., Jr.; Peralta, J. E.; Ogliaro, F.; Bearpark, M. J.; Heyd, J. J.; Brothers, E. N.; Kudin, K. N.; Staroverov, V. N.; Keith, T. A.; Kobayashi, R.; Normand, J.; Raghavachari, K.; Rendell, A. P.; Burant, J. C.; Iyengar, S. S.; Tomasi, J.;

Cossi, M.; Millam, J. M.; Klene, M.; Adamo, C.; Cammi, R.; Ochterski, J. W.; Martin, R. L.;
Morokuma, K.; Farkas, O.; Foresman, J. B.; Fox, D. J. Gaussian~16 Revision C.01. 2016;
Gaussian Inc. Wallingford CT.